Chapter 6

Gluon Propagator on Vortex-Modified Backgrounds

Here we present the results from the gluon propagator, calculated according to method outlined in Chapter 4, on our three vortex-modified configurations:

1. Original 'untouched' fields, $U_\mu(x)$,
2. Projected vortex-only fields, $Z_\mu(x)$,
3. Vortex-removed fields, $R_\mu(x) = Z_\mu^\dagger(x)\, U_\mu(x)$.

6.1 Preliminary Results

Calculating the scalar propagator on untouched, vortex-removed and vortex only configurations gives the results illustrated in Fig. 6.1. To make contact with the tree-level propagator at large q^2, we renormalise such that $q^2 D(q^2) = 1$ for $qa = 3.0$ on the original configurations, and apply this same renormalisation factor to the vortex removed and vortex only propagators. The vortex removed configurations display the expected behaviour, with vortex removal corresponding to significant infrared suppression of the propagator when compared to the untouched propagator, in agreement with the results of Ref. [64]. The increased roughness of the gauge fields after vortex removal is evidenced by the enhancement of the propagator at large q. This reflects the increase in short-distance fluctuations that have been introduced to the gauge fields by the vortex removal procedure.

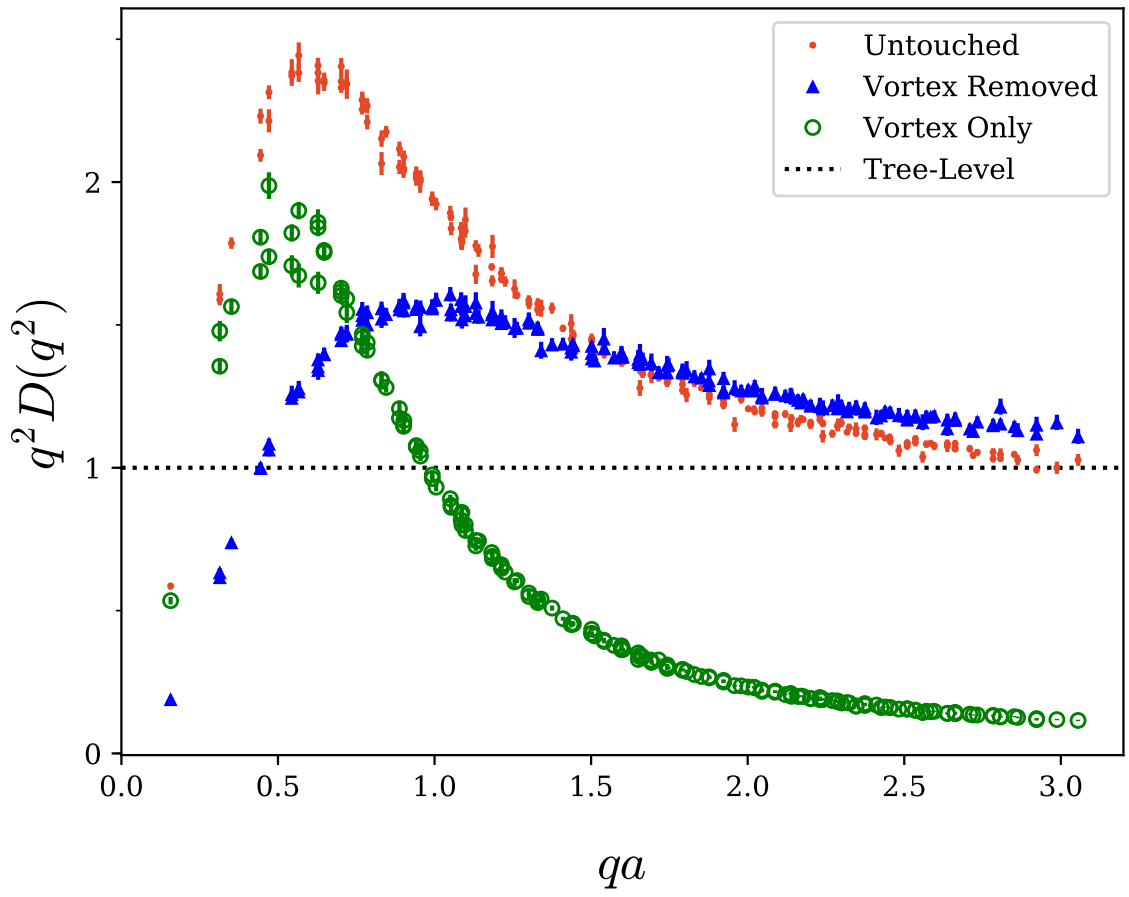

Fig. 6.1 The gluon propagator calculated from the original untouched (red dots), shown with the vortex removed (blue triangles) and vortex only (green open circles) results. Here, the renormalisation factor for the vortex removed and vortex only propagators is chosen to be the same as for the untouched propagator.

It is interesting to note that the vortex only propagator retains approximately two thirds of the untouched propagator's peak strength. This is comparable to previous work showing partial recovery of the string tension on vortex only configurations [53, 54, 65, 66]. Despite only recovering a portion of the original strength, the infrared peak is still considerably greater than the peak observed in the vortex removed propagator. The loss of strength is most likely in part because of the known imperfections in the vortex identification algorithm that results in some vortex matter remaining in the vortex removed configurations. The vortex only configurations also exhibit a loss of short range strength, due to the absence of the high frequency modes that are instead contained within the vortex removed field.

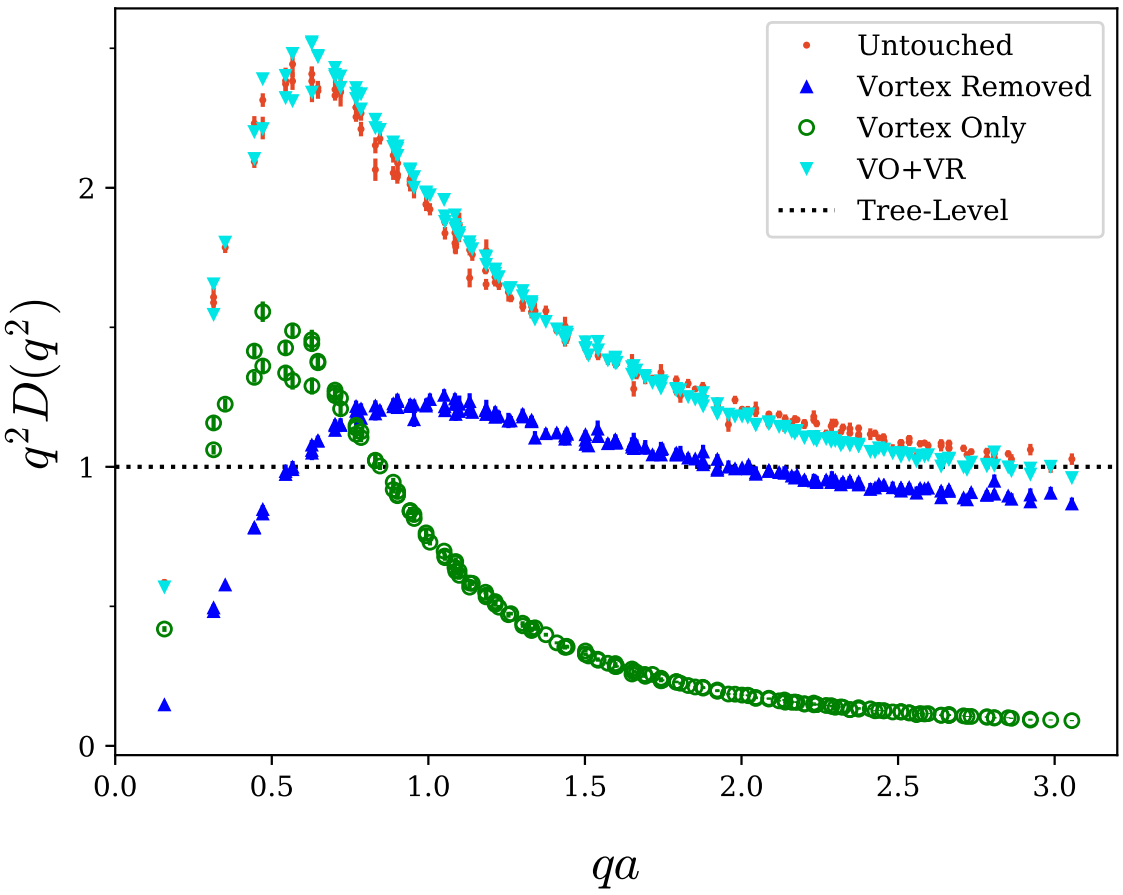

Fig. 6.2 The gluon propagator from the original untouched ensemble as in Fig. 6.1, now shown with the independently renormalised sum (cyan triangles) of the vortex removed and vortex only propagators. The two vortex modified propagators are also shown, but here their renormalisation factor is chosen to be the same as for the summed propagator.

If we sum the vortex only and vortex removed propagators and independently renormalise such that $q^2\,D(q^2) = 1$ at $qa = 3.0$, we obtain the result shown in Fig. 6.2. Here we observe agreement between the untouched and summed propagators. This indicates that vortex modification effectively partitions the lattice configuration into short range physics on the vortex removed configurations and long range physics on the vortex only configurations, up to errors in the vortex identification procedure.

6.1.1 Partitioning

This partitioning is expected if the vortex removed and vortex only configurations are orthogonal. To see how this behaviour emerges, suppose that we can decompose the

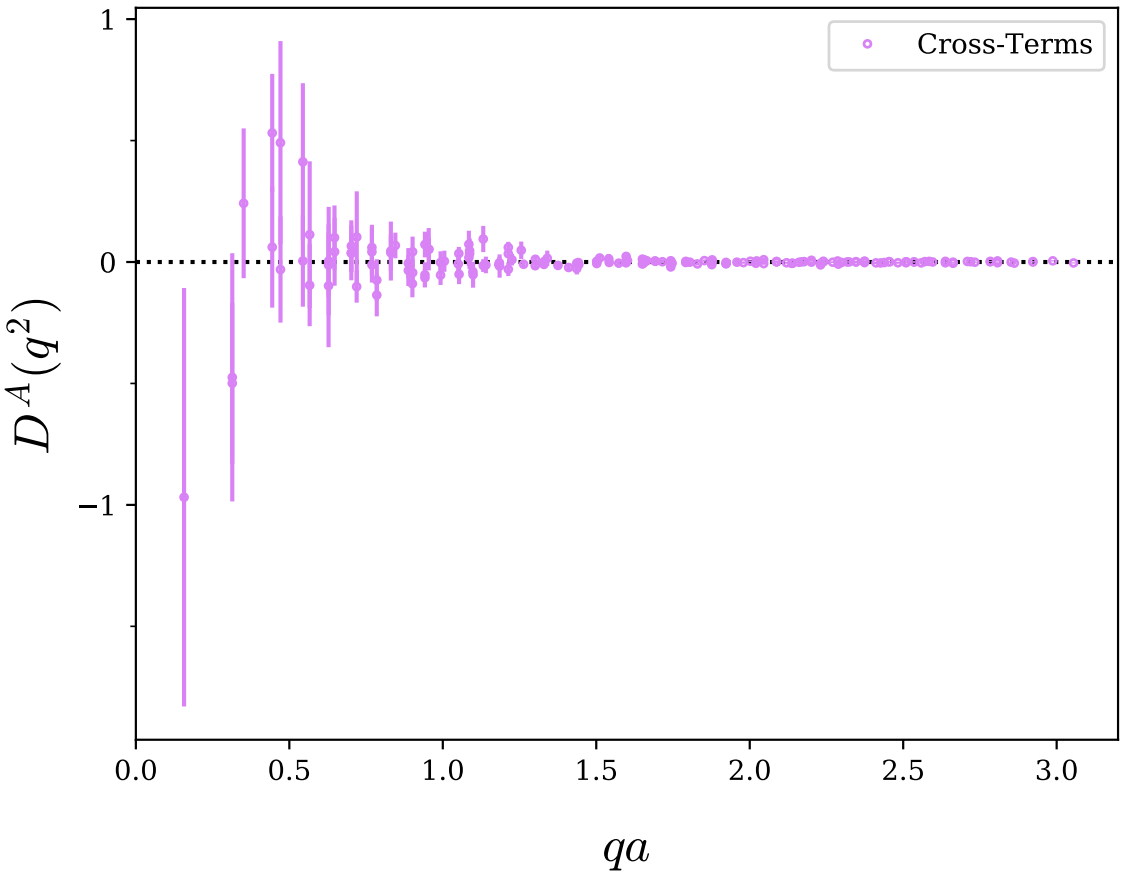

Fig. 6.3 Calculation of the cross-terms arising from Eq. 6.2

gluon field A_μ into two independent fields as follows

$$A_\mu(p) = B_\mu(p) + C_\mu(p). \tag{6.1}$$

In the context of this work, we associate B_μ with the background field of short-range gluon fluctuations and C_μ with the centre vortex field. Note also that if B and C are in Landau gauge then so is A. Using this partitioning it follows that the gluon propagator

for A can be written as the sum of the respective gluon propagators for B and C,

$$\begin{aligned} D^A_{\mu\nu}(p) &= \frac{1}{V}\langle A_\mu(p)\, A_\nu(-p)\rangle \\ &= \frac{1}{V}\Big(\langle B_\mu(p)B_\nu(-p)\rangle + \langle C_\mu(p)C_\nu(-p)\rangle \\ &\qquad + \langle B_\mu(p)C_\nu(-p) + C_\mu(p)B_\nu(-p)\rangle\Big) \\ &= D^B_{\mu\nu}(p) + D^C_{\mu\nu}(p), \end{aligned} \tag{6.2}$$

where we have made use of the fact that B and C represent orthogonal degrees of freedom in the gauge field and hence in the ensemble average the cross-correlations should vanish. These cross-correlations are explicitly calculated by evaluating

$$D_{\text{cross-terms}}(p^2) = \frac{2}{3\,(n_c^2-1)\,V}\,\langle \mathrm{Tr}\,(B_\mu(p)C_\mu(-p) + C_\mu(p)B_\mu(-p))\rangle\ , \tag{6.3}$$

analogous to the scalar gluon propagator derived in Chapter 4. The results of this calculation are shown in Fig. 6.3. As can be clearly seen, in the ensemble average Eq. 6.3 vanishes, indicating that the vortex only and vortex removed configurations truly do represent a orthogonal degrees of freedom.

To elucidate the connection to the unitary formulation of the lattice gauge links, we suppose that we can transform A to an "ideal centre gauge" such that in lattice units the field C consists purely of centre phases,

$$C_\mu(x) = k\,\frac{2\pi}{3}I, \quad k \in \{-1, 0, +1\}. \tag{6.4}$$

On a continuous manifold we can write the Wilson line corresponding to a lattice link as a path-ordered exponential,

$$U_\mu(x) = \mathcal{P}e^{\,i\int_0^1 d\lambda\, A_\mu(x+\lambda\hat{\mu})}. \tag{6.5}$$

The lattice midpoint approximation replaces the integral as follows,

$$U_\mu(x) = e^{iA_\mu(x+\hat{\mu}/2)}. \tag{6.6}$$

As $A = B + C$ it immediately follows that we can write

$$U_\mu(x) = e^{iB_\mu(x+\hat{\mu}/2)}\, e^{iC_\mu(x+\hat{\mu}/2)}, \tag{6.7}$$

noting that in our ideal centre gauge $[B, C] = 0$ so the Baker-Campbell-Haussdorff relation is trivial. Identifying

$$Z_\mu(x) = e^{iC_\mu(x+\hat{\mu}/2)} \tag{6.8}$$

as the vortex-projected field, and

$$R_\mu(x) = e^{iB_\mu(x+\hat{\mu}/2)} \tag{6.9}$$

as the background remainder field we thus recover the decomposition of the links used herein,

$$U_\mu(x) = Z_\mu(x) \cdot R_\mu(x). \tag{6.10}$$

In practise, on the lattice the maximal centre gauge fixing that is implemented will differ from the ideal centre gauge postulated here due to apparent numerical difficulties in simultaneously identifying all vortex matter within an $SU(3)$ gauge field. What this means is that the projected field Z may not capture all of the vortex matter such that there is some non-trivial topological structures that remain in the background field R. The infrared enhancement in the vortex removed results in Fig. 6.1 suggests this is the case.

6.1.2 Renormalisation

In Fig. 6.2 it proved necessary to independently renormalise the untouched and summed propagators such that they agree at $qa = 3.0$. The necessity of this renormalisation is worth discussing, as it is important to motivate why comparison between the original and reconstructed propagators is valid. To do this, it is beneficial to first consider the renormalised gluon propagator in the continuum. The renormalised propagator at any loop order, $D^{\mathrm{C}}_R(q^2)$ can be related to the bare propagator, $D^{\mathrm{C}}(q^2)$ via the relationship

$$D^{\mathrm{C}}(q^2) = Z_3^{\mathrm{C}}\, D^{\mathrm{C}}_R(q^2)\,. \tag{6.11}$$

Typically Z_3^{C} and $D^{\mathrm{C}}(q)$ are infinite, whereas $D^{\mathrm{C}}_R(q)$ is finite. The renormalised propagator is not independent of the renormalisation scheme, and the expression for Z_3^{C} depends on the renormalisation scheme employed. For example, in the minimal subtraction (MS) scheme at one-loop order with no quark fields, $Z_3^{\mathrm{C}} = 1 + \frac{5g^2}{8\pi^2\epsilon}$ [3], where the quantity ϵ is introduced during the analytic continuation to $d = 4 - \epsilon$ dimensions

as part of the dimensional regularisation procedure. However, regardless of the chosen renormalisation scheme, the renormalised propagator can always be expressed in the form shown in Eq. 6.11 [67].

On the lattice, we can explicitly calculate the now finite bare dimensionless propagator $D^{\mathrm{L}}(q^2)$, as the lattice introduces an explicit momentum cutoff of $\frac{\pi}{a}$. In the language of the continuum, this can be thought of as an approximation of the continuum bare propagator to all loop orders. Similarly, the lattice renormalisation constant $Z_3(\mu, a)$ is also finite. On the lattice, Eq. 6.11 becomes

$$a^2 D^{\mathrm{L}}(q^2) = Z_3(\mu, a)\, D_R(q^2)\,, \tag{6.12}$$

where the a^2 factor restores the dimensionality of the left-hand side of the equation. Despite the finiteness of $D^{\mathrm{L}}(q^2)$ and $Z_3(\mu, a)$, it is still necessary to enforce a renormalisation scheme to be able to draw meaningful comparisons between propagators. As such, we employ the momentum space subtraction (MOM) scheme [44, 68, 69], which requires that for some sufficiently large μ

$$D_R(q^2)\Big|_{q^2=\mu^2} = \frac{1}{\mu^2}\,. \tag{6.13}$$

This sets the value of the renormalisation constant to be

$$Z_3(\mu, a) = a^2\, \mu^2\, D^{\mathrm{L}}(\mu^2)\,, \tag{6.14}$$

such that

$$D_R(q^2) = \frac{D^{\mathrm{L}}(q^2)}{\mu^2\, D^{\mathrm{L}}(\mu^2)}\,. \tag{6.15}$$

This renormalised propagator is what we plot in e.g. Fig. 6.2. The value of μ is arbitrary, however it is necessary that it is sufficiently large such that it is outside the infrared region where the gluon propagator exhibits substantial deviation from tree-level behaviour. Furthermore, μ must be away from the momentum cutoff, as the renormalisation constant is only independent of the cutoff in the limit that the cutoff tends towards infinity [44, 70]. Given the momentum range of $qa \in [0, 4.6]$, arising from the momentum variables described in Sec. 4.2, a choice of $\mu = 3.0$ satisfies both conditions. Additionally, it also falls below the maximum momentum of $qa = 3.1$ imposed by the momentum half-cut described in Sec. 4.3. Once the renormalisation scheme has been imposed, it is then possible to connect the lattice results with those

obtained from perturbation theory by connecting the renormalisation constant with those obtained from the MS or modified minimal subtraction ($\overline{\text{MS}}$) schemes.

This discussion of renormalisation has motivated why it is acceptable to compare the untouched and summed propagators in Fig. 6.2; it is the renormalised propagator, not the bare propagator, that carries the physical meaning. Hence, the fact that the untouched and summed propagators agree after renormalisation is an important result indicating the effective partitioning of the gluon propagator under vortex modification. The final point worth discussing is the renormalisation applied to the vortex only and vortex removed propagators. Given that we don't have an *a priori* expectation of the tree-level behaviour, imposing the MOM condition lacks meaning. Instead, to facilitate comparisons, we make use of the original $Z_3(\mu, a)$ obtained for the untouched propagator unless specified otherwise. Maintaining this consistency is sufficient to comment on the qualitative shape of the propagator, which is the most significant point of interest in this research.

6.2 Impact of Cooling

After performing 10 sweeps of cooling on the untouched, vortex-removed and vortex-only ensembles, we obtain the results shown in Fig. 6.4. As is typical of cooling, the removal of short range structures means that all three ensembles tend to zero as $q \to \infty$. There is now a noticeable improvement in the agreement between the untouched and vortex only configurations; however there is still a difference present, especially in the $qa \approx 0.5$ and $qa \approx 1.5$ regions.

We perform the same analysis of the vortex only propagator under cooling as performed in Sec. 5.2 on the untouched propagator. Once again in gauge fixing, each sweep is preconditioned by the Landau gauge transformation of the previous sweep in descending order. The result of this analysis is shown in Fig. 6.5. This figure shows a similar change in the vortex only propagator when compared to the untouched propagator in Fig. 5.2, with an enhancement in the infrared and suppression in the UV modes. The UV suppression is less noticeable in this case due to the prior removal of short range effects brought about by the vortex identification.

We observe that the vortex only and untouched propagators in Fig. 6.4 resemble the gluon propagator under a differing number of sweeps of cooling, as shown in Fig. 5.2

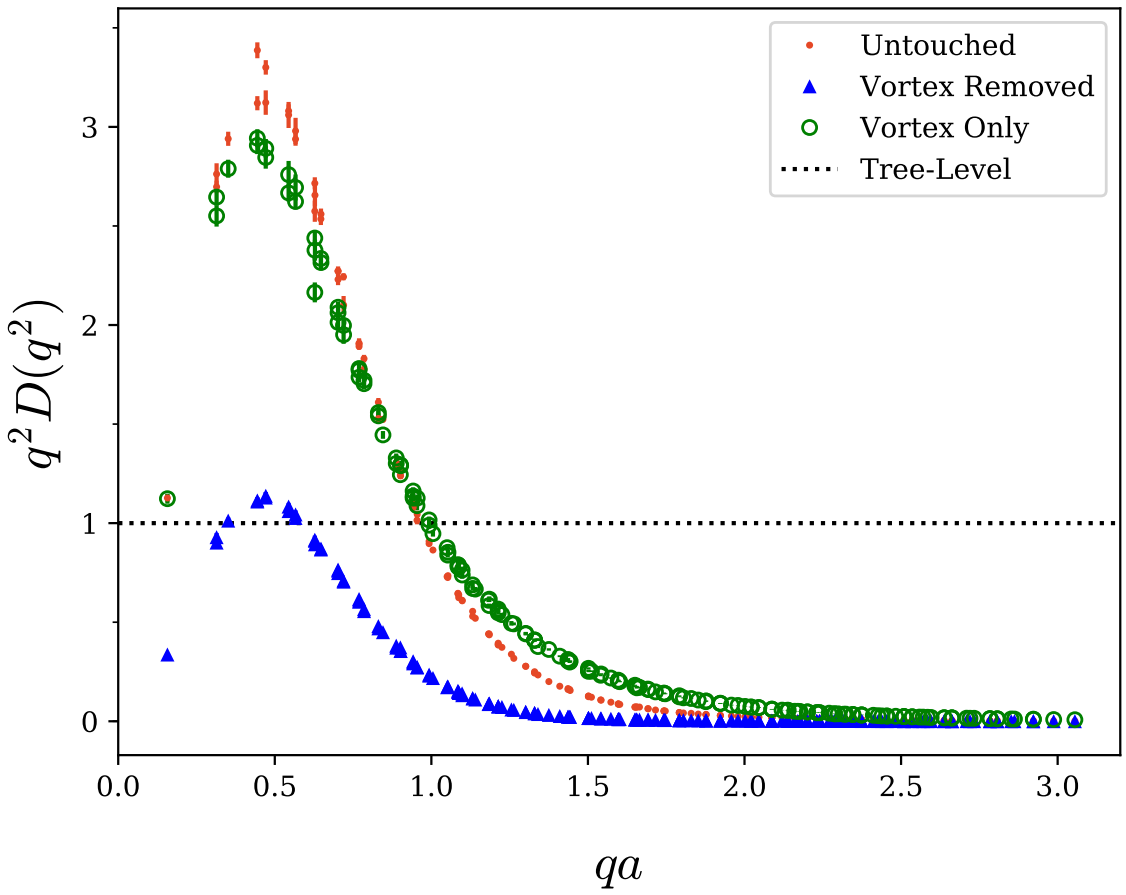

Fig. 6.4 The gluon propagator calculated on the three ensembles after 10 sweeps of cooling. We now observe an improved agreement between the untouched and vortex only propagators.

and Fig. 6.5. The vortex only propagator has a peak that sits below the untouched propagator, and the untouched propagator is further suppressed in the $qa \approx 1.5$ region. Following the trend in Fig. 5.2 and Fig. 6.5, this indicates that further cooling on the vortex only propagator would align it with the untouched propagator. This follows from an understanding that the vortex-only configurations are initially much rougher than their untouched counterparts [49], and should therefore require additional cooling to obtain agreement with the untouched configurations.

We take the average $\mathcal{O}(a^4)$ three-loop improved action of the lattice divided by the single instanton action $S_0 = \frac{8\pi^2}{g^2}$, denoted $\bar{S}/S_0$, to be a measure of roughness. We observe that for $n < 20$ cooling sweeps the vortex-only configurations have a significantly higher action than their untouched counterparts after the same number

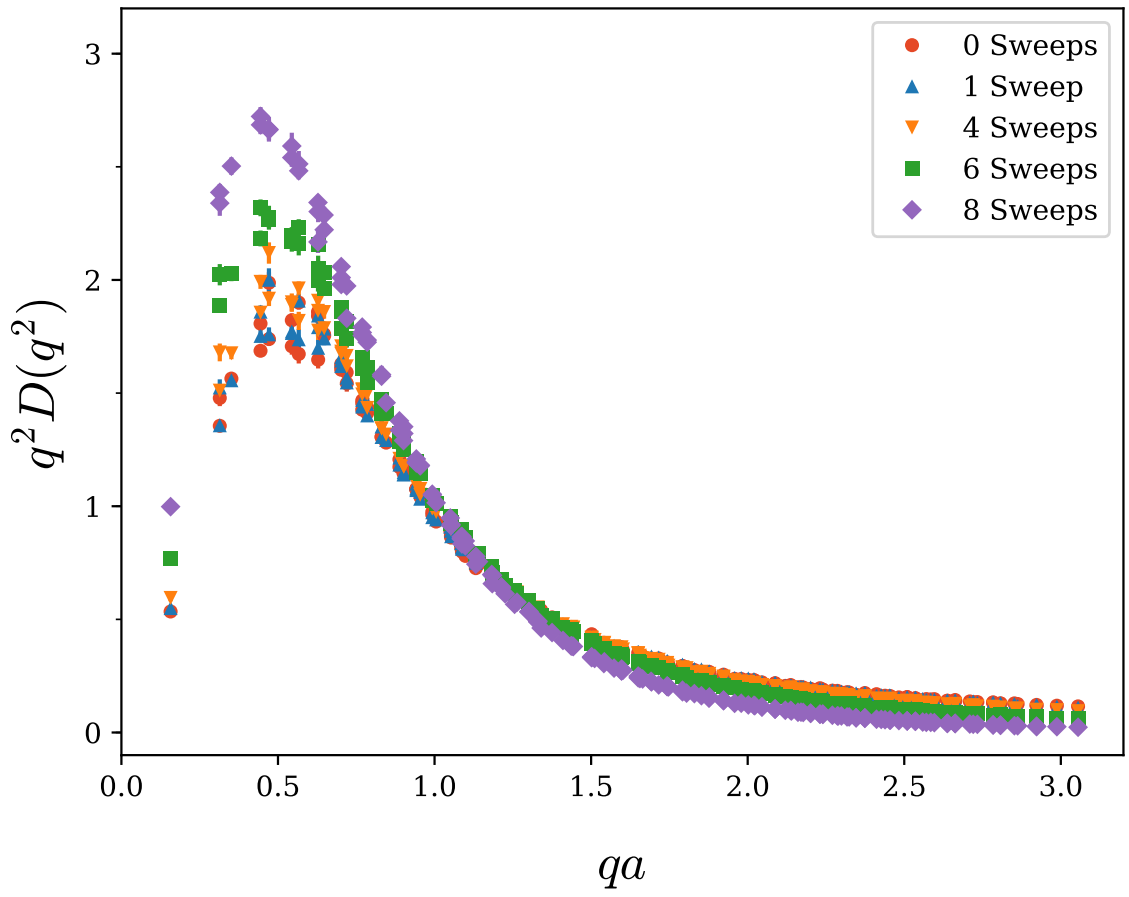

Fig. 6.5 The vortex only propagator after different sweeps of cooling. A trend similar to Fig. 5.2 is observed, with enhancement in the infrared and suppression in the UV region.

of sweeps of cooling, as illustrated in Fig. 6.6. We therefore seek to find the number of sweeps required to best match the action between the vortex-only and untouched configurations. The results of this procedure are shown in Table 6.1. If we now plot these matched configurations, we obtain the results shown in Fig. 6.7. Here we have truncated the plot at large qa to better show the agreement in the mid-qa region. By matching the actions as closely as possible with an integer number of cooling sweeps, we see that there is a better agreement between the untouched and vortex-only gluon propagators.

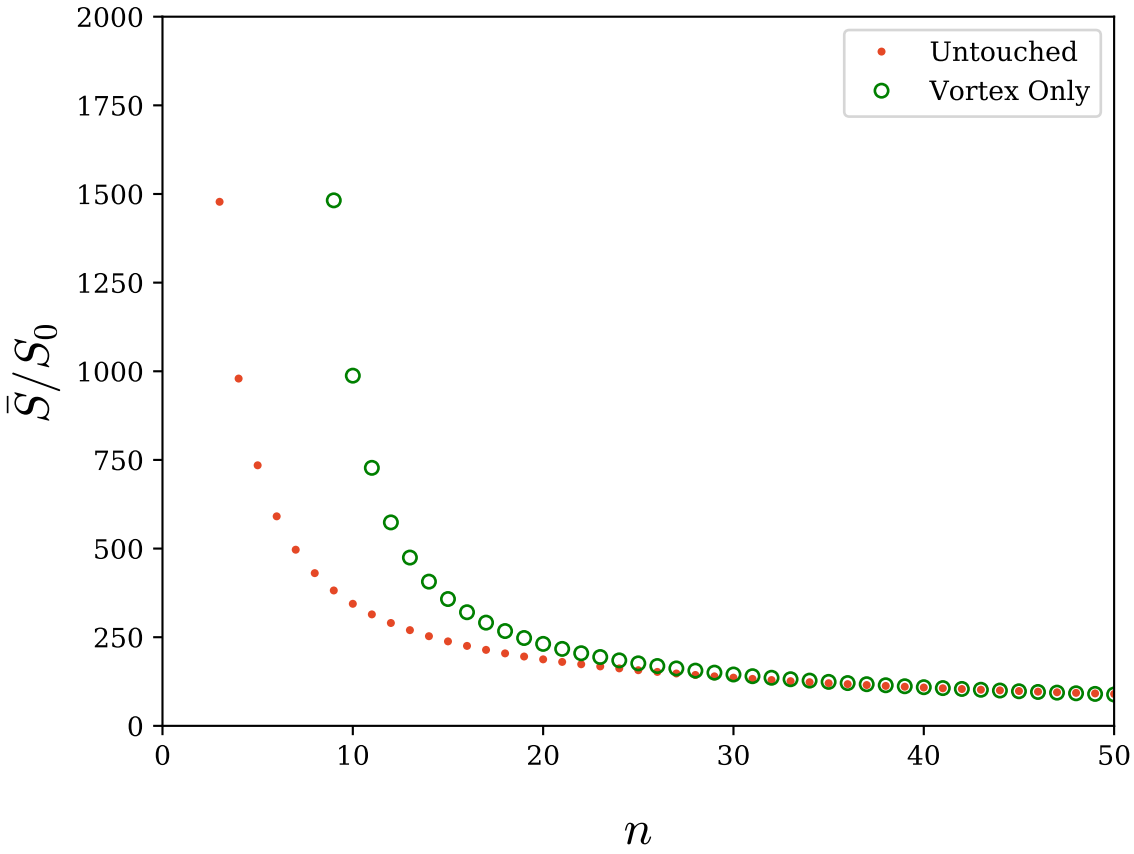

Fig. 6.6 The average action calculated on the untouched and vortex-only configurations as a function of cooling sweeps, n. The vortex only configurations are initially rougher than the untouched, as evidenced by the higher average action.

6.3 Summary

The results presented above concur with the now significant body of evidence that centre vortices contain the essential degrees of freedom of the Yang-Mills vacuum, such that the application of smoothing enables the recreation of the major features of QCD [40, 49, 53, 54, 71]. We have shown that vortex identification partitions the gluon propagator into low and high momentum modes, with the vortex only configurations encapsulating the majority of the infrared strength. Cross-correlation between the vortex only and vortex removed propagators can be seen to vanish in the ensemble average. By cooling the configurations, we observe that the vortex only configurations are continuously suppressed, while the infrared peak in the untouched and vortex only propagator acquires better agreement. By tuning the number of cooling sweeps to best match the average action of the vortex only and untouched configurations, we can

Table 6.1 Comparison of the number of cooling sweeps on the untouched (n_U) and vortex only (n_{VO}) configurations required to match the average action.

n_U	$\bar{S}/S_0$	n_{VO}	$\bar{S}/S_0$
5	734.83	11	727.67
10	344.22	15	357.68
15	238.21	20	231.19
20	187.55	24	184.68
25	156.92	28	155.72
30	135.91	32	135.61
35	120.29	36	120.66
40	107.08	40	109.02

effectively match the gluon propagators obtained from each of these configurations.

Noting that sufficient smoothing of a vortex-only field generates a topological background of instanton-like objects, we can regard the thin centre vortices as the seeds of instantons. The smoothing process that is applied on the vortex-only configurations raises a question regarding the precise role of vortices in the restoration of the infrared propagator; is it simply the presence of (sufficiently smoothed) vortices or is it more indirectly the reformation of the instanton background? If we examine Fig. 6.4, we see that after the application of 10 sweeps of cooling the vortex-only propagator has the appropriate qualitative infrared behaviour. Comparing with previous work, in particular Fig. 7 within Ref. [53] (replicated in Fig. 6.8) which shows the typical distribution of the instanton radius against the topological charge at the centre, we can see that after only 10 sweeps of cooling the vortex-only distribution still deviates significantly from the ideal theoretical instanton relationship. This suggests that it is the smoothed centre vortices that are directly responsible for the infrared structure of the gluon propagator.

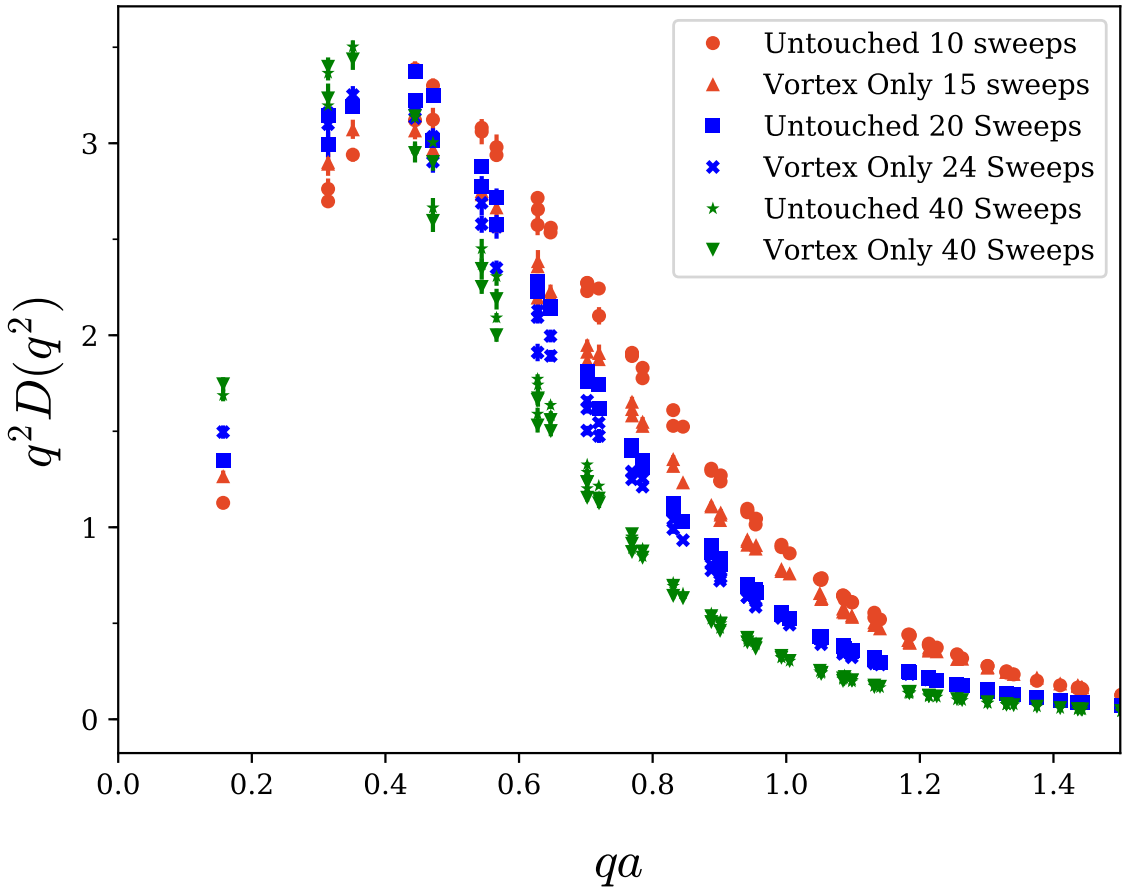

Fig. 6.7 Comparison of the gluon propagator on the untouched and vortex only configurations after tuning the number of cooling sweeps to best match the average plaquette action. This procedure gives a much better agreement in the shape of the gluon propagator from the two configurations.

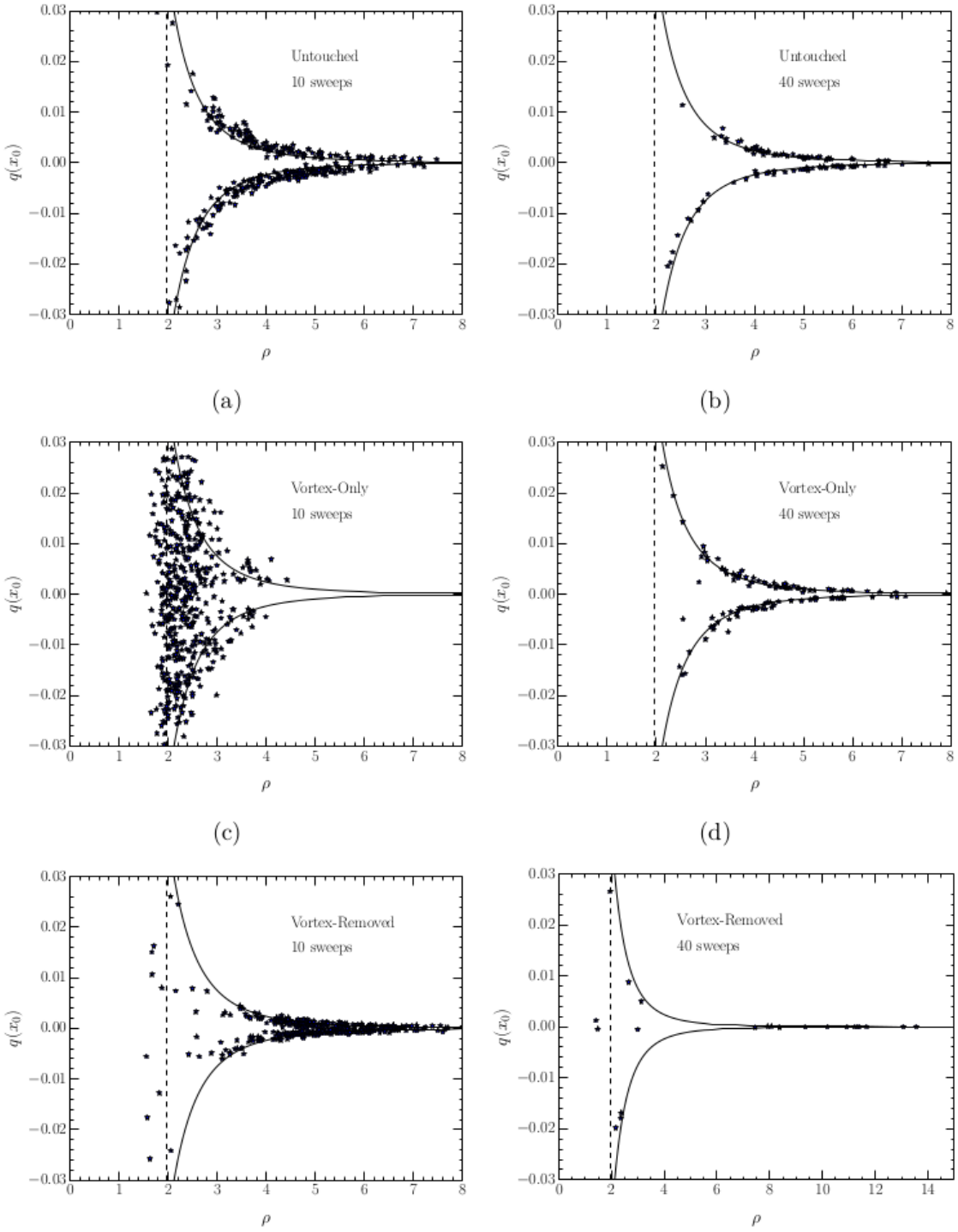

Fig. 6.8 The topological charge at the instanton centre, $q(x_0)$, is plotted against the instanton radius ρ for the vortex modified configurations under 10 and 40 sweeps of cooling. The solid line represents the theoretical distribution. These plots are acquired from Trewartha et al. [53].